Targeting Tn-antigen-positive human tumors with a recombinant human macrophage galactose C-type lectin

François Bulteau, Michel Thépaut, Maxime Henry, Amandine Hurbin, Laetitia Vanwonterghem, Corinne Vivès, Aline Le Roy, Christine Ebel, Olivier Renaudet, Franck Fieschi, et al.

molecular pharmaceutics

pubs.acs.org/molecularpharmaceutics

Article

Targeting Tn-Antigen-Positive Human Tumors with a Recombinant Human Macrophage Galactose C-Type Lectin

François Bulteau, Michel Thépaut, Maxime Henry, Amandine Hurbin, Laetitia Vanwonterghem, Corinne Vivès, Aline Le Roy, Christine Ebel, Olivier Renaudet, Franck Fieschi,* and Jean-Luc Coll*

Cite This: https://doi.org/10.1021/acs.molpharmaceut.1c00744

Read Online

ACCESS | Metrics & More | Article Recommendations | Supporting Information

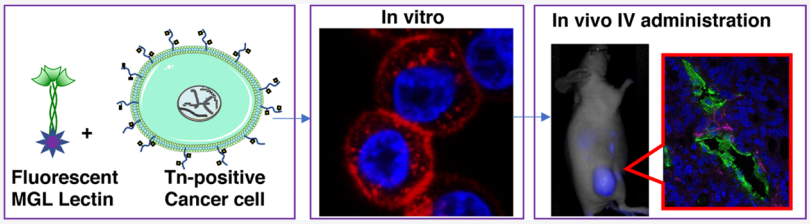

ABSTRACT: Alterations in glycosylation cause the emergence of tumor-associated carbohydrate antigens (TACAs) during tumorigenesis. Truncation of *O*-glycans reveals the Thomsen nouveau (Tn) antigen, an *N*-acetylgalactosamine (GalNAc) frequently attached to serine or threonine amino acids, that is accessible on the surface of cancer cells but not on healthy cells. Interestingly, GalNac can be recognized by macrophage galactose lectin (MGL), a type C lectin receptor expressed in immune cells. In this study, recombinant MGL fragments were tested *in vitro* for their cancer cell-targeting efficiency by flow cytometry and confocal microscopy and *in vivo* after administration of fluorescent MGL to tumor-bearing mice. Our results demonstrate the ability of MGL to target Tn-positive human tumors without inducing toxicity. This outcome makes MGL, a fragment of a normal human protein, the first vector candidate for *in vivo* diagnosis and imaging of human tumors and, possibly, for therapeutic applications.

KEYWORDS: *cancer, Tn antigen, C-type lectin*

INTRODUCTION

The external surface of prokaryotic and eukaryotic cells is typically covered by a dense and diversified array of glycans[1] resulting from complex enzymatic processes that generate polymeric sugars covalently linked to proteins or lipids;[2] these processes are frequently altered during oncogenic transformation, which leads to the appearance of tumor-associated carbohydrate antigens (TACAs) on cancer cells.[3] Common alterations are increased amounts of sialylated Lewis antigen and sialylated and polysialylated glycosylation, ectopic fucosylation leading to abnormal glycoconjugate levels, altered branching of *N*-glycans, and truncated *O*-glycans.[4,5]

The appearance of *N*-acetylgalactosamine (GalNAc) on the surface of cancer cells results from altered glycosylation.[6] The principal antigen harboring terminal GalNAc is the Thomsen nouveau (Tn) antigen (GalNAcαO-Ser/Thr), which is frequently detected in cancers (90% of carcinomas) but is not present or is masked on healthy cells.[7,8] The presence of this Tn antigen is caused by a mutation in the tumor-expressed *Cosmc* gene, which has been correlated with metastasis formation and poor prognosis.[9,10]

The role of the Tn antigen is not fully understood, but it is known that it can be recognized by macrophage galactose lectin (MGL) expressed in dendritic cells and macrophages. This recognition by immune cells can lead to immunosuppressive effects and may allow tumors to escape the surveillance of the immune system.[11−13]

Antibodies targeting the Tn antigen have been developed, but their specificity remains questionable,[14−16] and there are no ongoing clinical studies using these antibodies, to the best of our knowledge.[15] It is thus necessary to develop Tn-targeting molecules that can eventually be injected in patients.

The high selectivity and specificity of lectins, constituting a family of proteins capable of specifically and reversibly binding to certain carbohydrates without modifying them, makes them good candidates for cancer diagnostics, especially since most validated cancer biomarkers are glycoproteins.[17] Some lectins are currently used *in vitro* to detect altered glycosylation in cancers, such as *Lens culinaris* lectin and *Vicia villosa* lectin, which are both extracted from plants and validated by the FDA,[18,19] but because of their nonhuman origins, these lectins cannot be administered in humans.

Received: September 24, 2021
Revised: December 1, 2021
Accepted: December 2, 2021

In 1988, K. Drickamer's team[20] used the term C-type lectin to identify calcium (Ca^{2+})-dependent lectin receptors.[21] These lectins bind to sugars via a highly conserved carbohydrate recognition domain (CRD) and can be either soluble or membrane-bound. Membrane-bound lectins are composed of a cytoplasmic domain, a transmembrane region, and an extracellular domain (ECD), which includes the CRD and often an oligomerization domain (also called a neck). Macrophage galactose lectin (MGL, also named CLEC10A and CD301) is a receptor expressed on the surface of some dendritic cells (DCs) and macrophages.[22] Among C-type lectin receptors on immune cells, the canonic isoform of MGL recognizes *N*-acetylgalactosamine (GalNAc) with high affinity,[11] while different splice variants of MGL can more broadly recognize ligands.[23] The other unique example of a specific lectin for GalNAc is the asialoglycoprotein receptor (ASGPR), which is specifically expressed in liver cells.[24]

In this study, we generated and characterized recombinant MGL fragments and tested them first *in vitro* for their Tn-specific cell targeting efficiency. We then investigated the ability of MGL to diffuse inside three-dimensional (3D) cultured spheroids. Finally, we demonstrated the specific labeling of tumors engrafted in mice after intravenous administration of a near-infrared fluorescent MGL.

MATERIALS AND METHODS

Production of MGL Constructs. The extracellular domain (ECD) of MGL, residues 61−292, was produced as previously described.[25]

The MGL carbohydrate recognition domain (CRD) was based on the smaller sequence corresponding to residues 156 to 292 only inserted in pET30b with an N-terminal His-Tag followed by a TEV proteolytic site. MGL CRD was expressed in *Escherichia coli*BL21(DE3) in 1 L of Luria broth (LB) medium supplemented with 50 μg/mL kanamycin at 37 °C. Expression was induced for 3 h with 1 mM isopropyl 1-thio-D-galactopyranoside (IPTG) when the culture reached an $OD_{600\ nm}$ of 1.2−1.5. The protein was expressed in the cytoplasm as inclusion bodies. Cells were pelleted by a 20 min centrifugation at 2000*g* at 4 °C. The pellet was resuspended in 30 mL of buffer 25 mM Tris−HCl pH 8, 150 mM NaCl, 4 mM $CaCl_2$, and one antiprotease tablet (cOmplete, ethylenediaminetetraacetic acid (EDTA) free Protease inhibitor cocktail, Roche). Bacteria were disrupted by sonication, and cell debris was eliminated by centrifugation at 100 000*g* for 1 h at 4 °C. The pellet was resuspended, washed, and recovered by centrifugation (100 000*g* for 30 min at 4 °C) two times using successively 30 mL of buffer 25 mM Tris−HCl pH 8, 150 mM NaCl, 2 mM urea, and 1% Triton and then 30 mL of buffer A with 0.01% β-mercaptoethanol.

Then the resulting inclusion body pellet was finally solubilized with 2 M ammonium hydroxide. The sample was centrifugated at 100 000*g* for 30 min at 4 °C and the MGL concentration adjusted at 2 mg/mL with 2 M ammonia, using MGL ECD $\varepsilon(280)$ = 63 430 M^{-1} cm^{-1}. The refolding is conducted by a global 10-fold dilution by a drop-by-drop addition within buffer 25 mM Tris−HCl pH 7.5, 500 mM NaCl, 25 mM $CaCl_2$. The protein solution is then dialyzed against 10 volumes of C buffer exchanged three times. Insoluble proteins were eliminated by centrifugation at 100 000*g* for 1 h at 4 °C. The protein was purified on HisTrap HP column GE Healthcare, eluted with buffer 25 mM Tris pH 8, 150 mM NaCl, 4 mM $CaCl_2$, 200 mM imidazole. Fractions containing the protein of interest were selected and dialyzed against buffer 25 mM Tris pH 8, 4 mM $CaCl_2$ and at the same time, the poly-histidine tag was cleaved off with TEV protease (1 mg for 6 mg of protein at 4 °C). Protein was further purified onto ion-exchange chromatography column (Mono Q 5/50 GL, GE-Healthcare), eluted within a 20 mL linear gradient of NaCl between A buffer 25 mM Tris pH 8, 4 mM $CaCl_2$ and B buffer 25 mM Tris pH 8, 4 mM $CaCl_2$, 1 M NaCl, from 0 to 100% of B. Active protein was selected with a GalNAc-Agarose affinity column (Sigma) and eluted with buffer 25 mM Tris−HCl pH 8, 150 mM NaCl, 10 mM EDTA. The protein pool containing protein of interest was then loaded onto a 125 mL Toyopearl HW-50S size exclusion column (Tosoh Bioscience) equilibrated in buffer 25 mM Tris−HCl pH 8, 150 mM NaCl, 4 mM $CaCl_2$. Eluted fractions were analyzed by sodium dodecyl sulfate polyacrylamide gel electrophoresis (SDS-PAGE) (12%), and fractions containing ECD were pooled and concentrated using a 5 kDa molecular weight cutoff (MWCO) ultrafiltration membrane.

Characterization of ECD and CRD Affinity by Surface Plasmon Resonance (SPR). SPR experiments were performed on a Biacore T200 using a CM3 series S sensor chip. Flow cells were activated as previously described.[26] Flow cell 1 was functionalized with bovine serum albumin (BSA), blocked with ethanolamine, and subsequently used as a control surface. Flow cells 2 and 3 were functionalized with 30 μL of BSA-GalNAc (60 μg/mL) in 10 mM NaOAc pH 4 and blocked with ethanolamine. The final densities on flow cells 2 and 3 were about 2900 RU. MGL ECD was injected at different concentrations ranging from 9 μM to 1.2 nM. Injections were performed at 20 μL/min using 25 mM Tris−HCl pH 8, 150 mM NaCl, 4 mM $CaCl_2$, 0.05% P20 surfactant as running buffer. Association time was 250 s, and dissociation time was 150 s. The surface was regenerated by the injection of 50 mM EDTA for 10 s at 100 μL/min. The data were analyzed with Biacore BIAevaluation software using a steady-state affinity model for K_d determination.

Analytical Ultracentrifugation. Sedimentation velocity experiments were performed at 42 000 rpm (130 000*g*) and 4 °C, on an analytical ultracentrifuge XLI, with a rotor Anti-60 (Beckman Coulter, Brea) and double-sector cells of optical path-length 0.15 or 1.2 cm equipped of Sapphire windows (Nanolytics, Potsdam, DE). The reference buffer was 25 mM Tris pH 8, 150 mM NaCl, 4 mM $CaCl_2$. Acquisitions were made using absorbance at 280 nm, and interference (655 nm) optics. Data were processed with REDATE v1.0.1 and then analyzed with SEDFIT v16.1 for $c(s)$ analysis.[27,28] Data resulting from SEDFIT analysis were exported to GUSSI v 1.3.2 for integration and figures.[29] The Svedberg equation was used to analyze the values of the sedimentation coefficient, s

$$s = M(1 - \rho\bar{v})/N_A 6phR_H$$

with M the molar mass, ρ and η the buffer density and viscosity, respectively, N_A Avogadro's number, and $R_H = R_0 f/f_0$ the hydrodynamic radius, where R_0 is the radius of the anhydrous volume and f/f_0 is the frictional ratio.

Buffer density (1.007 g/mL) and viscosity (1.601 cP) were calculated with SEDNTERP v 20130813 β.[30] For MGL ECD, M = 23160 Da and $\bar{v}$ = 0.706 mL/g were calculated from sequence with SEDFIT.

Labeling of MGL ECD with Alexa Fluor 680. MGL ECD was dialyzed against 20 mM 4-(2-hydroxyethyl)-1-piperazineethanesulfonic acid (HEPES) pH 8, 150 mM NaCl, 4 mM

https://doi.org/10.1021/acs.molpharmaceut.1c00744
Mol. Pharmaceutics XXXX, XXX, XXX−XXX

$CaCl_2$ to eliminate Tris. MGL ECD at 5.3 mg/mL was labeled with Alexa Fluor 680 NHS Ester (succinimidyl ester) (Thermo Fisher Scientific) at 0.5 mg/mL for 2 h at room temperature and 4 h at 4 °C. After labeling, the mixture was dialyzed against 20 mM HEPES pH 7.4, 150 mM NaCl, 4 mM $CaCl_2$ to discard the excess of Alexa Fluor 680. The degree of labeling of the protein was calculated to 0.8 using the following formula

$$\text{degree of labelling} = \frac{A_{680\text{nm}}}{[\text{protein}] \times \varepsilon_{\text{dye}}}$$

The labeled protein was purified from the reaction mixture by size exclusion chromatography on a Toyopearl HW-50S column (Tosoh Bioscience) and eluted with 20 mM HEPES pH 7.4, NaCl 150 mM, 4 mM $CaCl_2$.

Cell Lines and 2D Cell Culture Conditions. HT29 is an epithelial cell line of human colon cancer (ATCC HTB-38). The cells were maintained in McCoy's 5A (Gibco—Life Technologies) medium supplemented with 10% of inactivated fetal bovine serum (FBS) (Dutscher) and kept at 37 °C in a 5% CO_2 humidified atmosphere.

A549 (epithelial cell line of carcinoma lung cancer (ATCC CCL-185)) and H322 (bronchioalveolar carcinoma, non-small cell lung cancer, ATCC CRL-5806) cell lines were maintained in RPMI medium (Gibco—Life Technologies) supplemented with 10% of inactivated FBS and kept at 37 °C in 5% CO_2 humidified atmosphere.

3D Culture of Spheroids. HT29 spheroids were created by plating HT29 (25 000 cells/well) cells into 96-well round-bottom ultra-low attachment spheroid microplates (Corning, Tewksbury, MA). The spheroid culture was maintained in McCoy's 5A medium with 10% FBS in a humidified atmosphere with 5% CO_2. Spheroid growth was monitored by microscopic examination with an inverted microscope.

Evaluation of Tn Expression by Flow Cytometry. Cells were grown and harvested at 70% confluency. The cells were washed with phosphate-buffered saline (PBS) 1× (Gibco—Life Technologies) and resuspended with Trypsin-EDTA (Gibco—Life Technologies). A total of 1 million cells were rinsed in PBS + 10% FBS and then incubated with an anti-CD175 mouse monoclonal antibody (Bric111, Thermo Fisher Scientific) with a 1/50 dilution for 1 h at room temperature. After rinsing in PBS, the cells were incubated with a secondary anti-mouse Ig1 antibody conjugated with Alexa Fluor 488 with a 1/250 dilution for 1 h at room temperature. Then, the cells were washed with PBS and analyzed by flow cytometry (Accuri C6 BD).

For HPA staining, cells were grown and harvested as previously described. Resuspended cells were washed with PBS 1× and labeled with different concentrations of HPA-Alexa Fluor 647 (Thermo Fisher Scientific) (0; 0.005; 0.001; 0.005; 0.01 μM) for 30 min at room temperature. The cells were washed with PBS 1× and analyzed by flow cytometry (Accuri C6, BD).

Labeling of Cells by MGL for Flow Cytometry and Microscopy. Cells were grown and harvested as previously described. Resuspended cells were washed with buffer 20 mM HEPES pH 7.4, 137 mM NaCl, 2 mM $CaCl_2$, 4 mM KCl and labeled with different concentrations of MGL ECD-Alexa Fluor 680 (0; 0.01; 0.05; 0.1; 0.5 μM) for 30 min at room temperature. The cells were washed with buffer 20 mM HEPES pH 7.4, 137 mM NaCl, 2 mM $CaCl_2$, 4 mM KCl and analyzed by flow cytometry (Accurry C6 BD).

For confocal microscopy, 500 000 H322 cells and 125 000 HT29 or A549 cells per well were plated in a four-well Nunc Lab-Tek II chambered coverglass (Thermo Fisher Scientific) for 24 h at 37 °C and then incubated with MGL ECD-Alexa Fluor 680 at different concentrations (0.05; 0.1; 0.5 μM) in 1 × PBS with 2 mM $CaCl_2$ for 30 min at room temperature. After rinsing, the cell nuclei were labeled with 20 μM Hoescht 33342 for 15 min at room temperature and washed with PBS. The cells were then observed immediately or after 2 h using a confocal microscope LSM710 NLO (Zeiss AxioObserver Z1) with a 63×/1.4 oil immersion objective.

Confocal Microscopy on Spheroids. The spheroids were labeled with MGL ECD-Alexa Fluor 680 for 0.5, 2, and 24 h at room temperature at different concentrations (0.1; 0.5; 1.0; and 5.0 μM). After three washes with TBST, the spheroids were fixed in 4% paraformaldehyde, included in Tissue-Tek optimum cutting temperature (O.C.T.), and cut with a cryostat (Leica) in 7 μm slices. Slices were washed with TBST, labeled with 5 μM Hoescht 33 342, and prepared under a coverslip with a drop of mounting medium (ROTIMount FluorCare, Roth). Spheroids were observed using a confocal microscope LSM710 NLO (Zeiss Axiovert Z1) and a 20× objective.

Labeling of Subcutaneous Tumor in Mice. All animal studies were performed in accordance with the European Economic Community guidelines and the "principles of laboratory animal care" and were approved by the institutional guidelines and the European Community (EU Directive 2010/63/EU) for the use of experimental animals (authorization for the experiment: APAFIS).

Six-week-old female NMRI nude mice (Janvier Labs, Le Genest-Saint Isle, France) were anesthetized using 4% isoflurane/air for anesthesia induction and 1.5−2% to maintain anesthesia. HT29 cells (5 million) were implanted subcutaneously in 250 μL PBS 1×. Tumor size was measured three times a week using a caliper, and the tumor volume was calculated as follows

$$\text{lenght} \times (\text{width})^2 \times 0.4$$

After 35 days, the mice were injected in the tail vein with 200 μL MGL ECD-Alexa Fluor 680 at 50 μM in HEPES buffer and were imaged using the LI-COR Pearl small animal imaging system at 700 nm.

Histology of Tumors. Tumors were removed and frozen in liquid nitrogen in the presence of optical coherence tomography (OCT). Frozen sections (7 μm) were fixed with 4% paraformaldehyde pH 7 for 5 min, washed three times in TBST, and then incubated in PBS + 5% goat serum for 30 min. After rinsing, the slices were labeled with a rat anti-mouse CD31 diluted 500 times (Pharmingen) for 24 h at 4 °C in a humidified atmosphere. They were then washed with TBST three times and incubated with a goat anti-rat IgG antibody conjugated with Alexa Fluor 488 (Invitrogen) for 1 h at room temperature. After two washes, tumors were counterstained with 1 μg/mL Hoescht 33 342 and mounted. The tumors were observed using a confocal microscope LSM510 NLO (Zeiss Axiovert Z1) and a 20x objective.

Statistical Analyses. All statistical analyses were proceeded with Statistica (StatSoft, Europe, Hamburg). Results of flow cytometry were expressed as mean ± standard deviation (SD). These data were analyzed for the 3 cell lines (HT29, A549, H322), for 5 MGL ECD concentrations (0, 0.01, 0.05, 0.1, and 0.5 μM), by repeated-measures analysis of variance (ANOVA).

https://doi.org/10.1021/acs.molpharmaceut.1c00744
Mol. Pharmaceutics XXXX, XXX, XXX−XXX

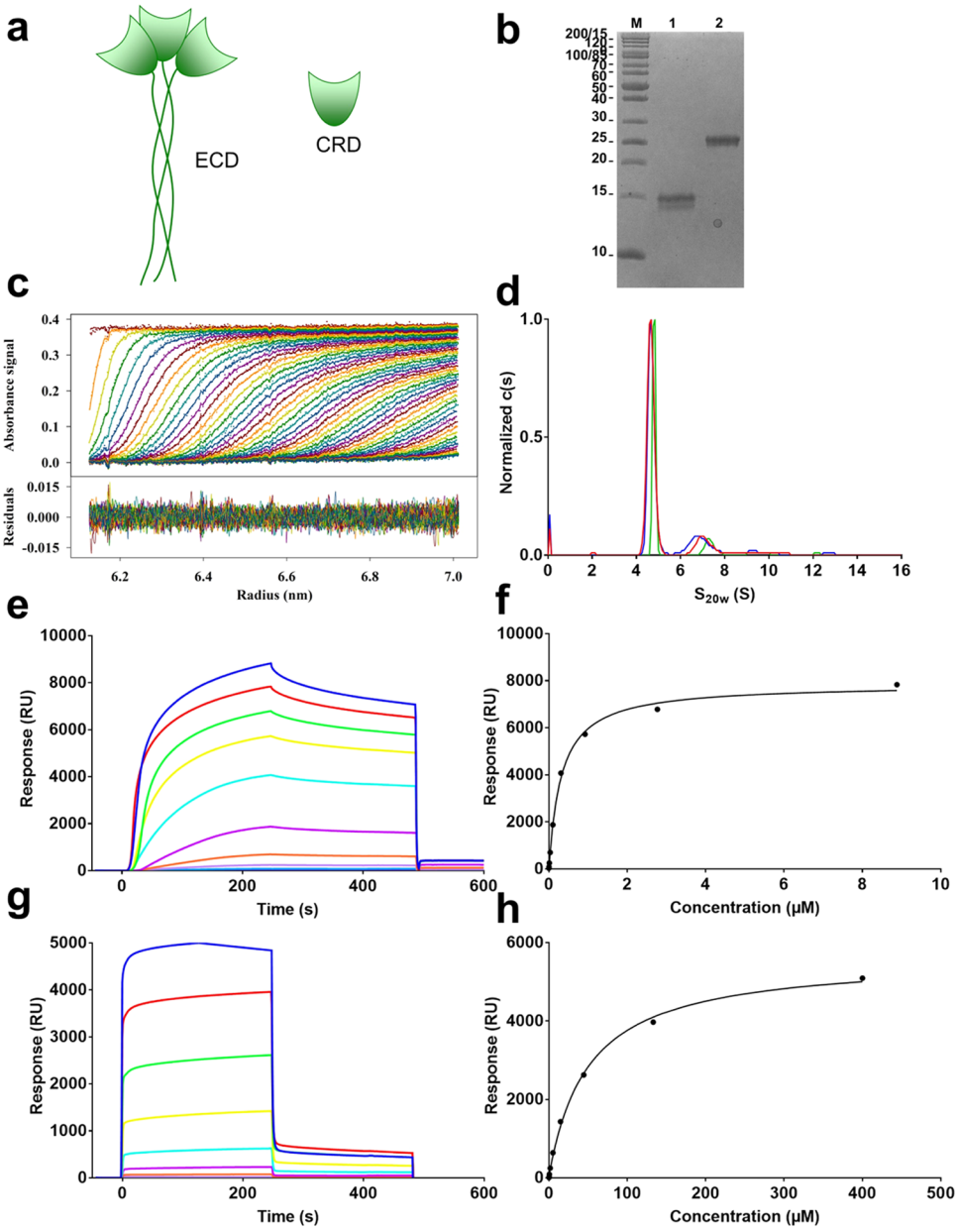

Figure 1. Expression, purification, and characterization of MGL. (a) Presentation of two different forms of MGL, CRD: carbohydrate recognition domain; ECD: extracellular domain (CRD + neck). (b) SDS-PAGE analysis of purified ECD and CRD. Lane 1: a unique band at ∼15 kDa corresponding to pure CRD is observed. Lane 2: a unique band at ∼28 kDa corresponding to pure ECD is observed. M: PAGE-ruler unstained protein ladder (fermentas). (c) Analytical ultracentrifugation analysis: superposition of selected experimental and fitted sedimentation velocity profiles (top), and residuals of the fit (bottom), obtained, in absorbance at 280 nm, every 10 min, and up to 8 h, at 130 000*g* and 4 °C. (d) Analytical ultracentrifugation analysis: Normalized $c(s)$, in absorbance for MGL ECD at 4 μM (red), 40 μM (blue), and 80 μM (green). (e, f) Surface plasmon resonance characterization of MGL constructs binding properties. (e) MGL ECD titration (threefold dilution series between 0.0013 and 8.9 μM) over a BSA-GalNAc Surface (2886 RU) reference surface-corrected sensograms. (f) Plots of MGL ECD binding responses as a function of their concentration by steady-state affinity model (black circles). (g) MGL CRD titration (threefold dilution series between 0.02 and 400 μM) over a BSA-GalNAc Surface (2886 RU) reference surface-corrected sensograms. (h) Plots of MGL CRD binding responses as a function of their concentration by steady-state affinity model (black circles).

Competition data were analyzed, using a range of 7 GalNAc concentrations (0, 0.01, 0.05, 0.1, 0.5, 5 μM, and negative control), by repeated-measures ANOVA. Post hoc comparisons were performed using pairwise *t*-tests between critical conditions (α = 0.05, two-tailed).

RESULTS

Production and Characterization of hMGL Recombinant Constructs. There are two isoforms of human MGL, which are results of alternative splicing. The most studied isoform is isoform 2, which was initially identified in macrophages.[31] In MGL isoforms 1 to 2, the carbohydrate recognition domain is identical, and no difference in carbohydrate specificity is thus anticipated. Differences between isoforms include a size difference of the oligomerization domain, with isoform 2 being shorter. Since isoform 2 is the better-characterized variant, we first studied this isoform. We cloned both the MGL carbohydrate recognition domain

https://doi.org/10.1021/acs.molpharmaceut.1c00744
Mol. Pharmaceutics XXXX, XXX, XXX−XXX

(CRD) and MGL extracellular domain (ECD) (Figure 1a). These two constructs were expressed in *E. coli* as inclusion bodies. They were refolded and purified as described in the experimental section. While the MGL CRD consists of a 15 kDa monomer (Figure 1b), the MGL ECD is larger (28 kDa) and can oligomerize due to its coiled−coiled oligomerization domain, providing an important avidity effect.[32] Sedimentation velocity-analytical ultracentrifugation (SV-AUC) was performed to determine the oligomerization status of MGL ECD. The sedimentation profiles obtained at 4, 40, and 80 μM showed the main contribution at s_{20w} = 4.8 S. Noninteracting species (NIS) appeared at a molar mass (M) of 79 ± 6 kDa. Combining the s-value and the molar mass from the NIS analysis, MGL ECD was identified as an elongated trimer (f/f_{min} =1.59) (Figure 1c,d). In the rest of the study, we will use the term MGL ECD to define the trimer. To characterize the affinity of both the CRD and MGL ECD constructs, we used surface plasmon resonance (SPR). Surfaces were functionalized with BSA-GalNAc, and a range of MGL ECD and MGL CRD concentrations were injected (Figure 1e−h). We observed that the signal increased with increasing concentration of MGL (Figure 1e,g) and was abolished in the presence of EDTA. To determine the dissociation constant (K_d), we plotted the data using a steady-state model (Figure 1f−h), and an apparent K_d of 50 μM was obtained for the MGL CRD, while an apparent $K_{d,app}$ of 316 nM was estimated for the MGL ECD construct. This difference between both constructs (by a factor greater than 150-fold) reflects the avidity effect generated by the trimerization within the MGL ECD and encouraged us to use this construct to target the Tn antigen directly on cells.

Tn Antigen Recognition on Whole Cells Using MGL ECD. To perform these experiments, we labeled the MGL ECD with Alexa Fluor 680. Considering previous work from Lescar et al.[33] and using *Helix pomatia* lectin (HPA), which recognizes the Tn antigen, we selected three cell lines expressing different Tn antigen levels. These cell lines, HT29, A549, and H322, presented high, low, and no Tn antigen on their surfaces, respectively (Table 1); this finding is consistent with that

Table 1. Labeling of Different Cancer Cell Lines by Different Proteins (Antibody against CD175 (Tn), MGL ECD, and *Helix pomotia* Lectin)

cell lines	origin	antibody bric111	MGL ECD	HPA
HT29	human colon cancer	+++	+++	+++
A549	human non-small cell lung cancer	+/−	+/−	−
H322	human non-small cell lung cancer	−	−	−

described in the literature with respect to HT29.[34,35] All FACS analyses were performed in parallel with the fluorescent anti-Tn antibody Bric111 and HPA to validate MGL staining.

As expected, important labeling was achieved with the positive HT29 cell line using three staining methods. A549 cells provided weak signals with the Bric111 antibody stain and MGL ECD-Alexa Fluor 680, while no detectable labeling was obtained with HPA. For the H322 cell line, no signal was detected for the three markers, as expected. The labeling of cells with MGL ECD-Alexa Fluor 680 is slightly enhanced with increasing concentrations of calcium (data not shown). Thus, the results obtained with the MGL ECD construct were as efficient as those obtained with the Bric111 antibody.

The cell lines were then labeled with increasing doses of MGL ECD-Alexa Fluor 680 and analyzed by flow cytometry. As shown in Figure 2a, the positive labeling of HT29 and A549

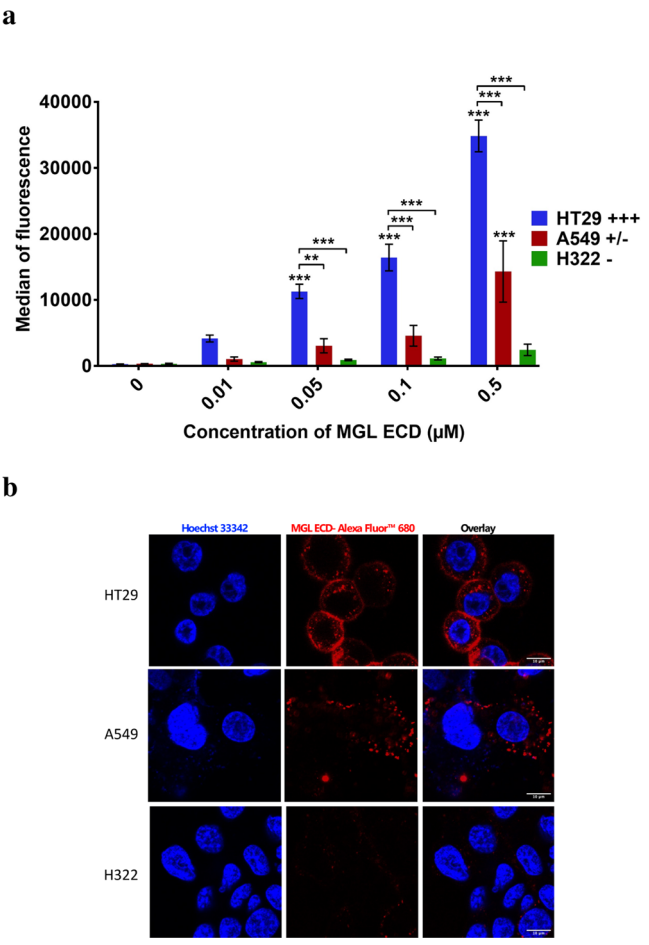

Figure 2. Labeling of three cancer cell lines by MGL ECD-Alexa Fluor 680. (a) Histogram of median of fluorescence ± SD in flow cytometry (n = 3). Stars on the histograms show the significance in relation to the concentration 0. Stars on the braces show a significant difference in cell lineage. *: p < 0,05; **: p < 0,001; ***: $p < 10^{-5}$. (b) Observation of HT29, A549, and H322 after MGL ECD-Alexa Fluor 680 labeling (0.5 μM, 2 h) by confocal microscopy. Red: Alexa Fluor 680 fluorescence; blue: Hoechst 33342 staining of nuclei. Scale bar: 10 μm.

cells increased with increasing MGL ECD-Alexa Fluor 680 concentration, without no saturation effect up to the highest tested concentration (0.5 μM). In addition, no labeling was detected on the H322 negative control cells except for a very weak signal obtained at the highest tested concentration (0.5 μM). These results were confirmed using confocal microscopy (Figure 2b). The HT29 cells were intensely labeled on the cell membrane and in the cytoplasm after 2 h of incubation with antibody, and the A549 staining was less intense. This finding suggested progressive intracellular accumulation of the bound MGL ECD-Alexa Fluor 680 constructs during the 2 h of incubation. Testing the H322 cell line, we found that MGL ECD-Alexa Fluor 680 binding was negligibly detectable.

To complete this experiment, we performed a competition assay. Fluorescent MGL ECD-Alexa Fluor 680 (0.05 μM) was

https://doi.org/10.1021/acs.molpharmaceut.1c00744
Mol. Pharmaceutics XXXX, XXX, XXX−XXX

incubated with HT29 cells in the presence of increasing concentrations of soluble GalNAc (Figure 3). The increase in

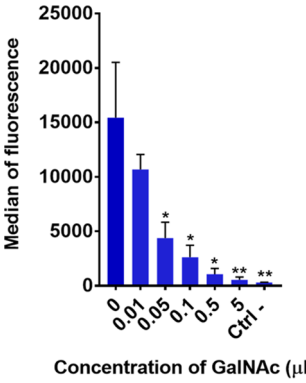

Figure 3. Competition assay. HT29 cells were incubated with MGL ECD-Alexa Fluor 680 in the presence of increasing concentrations of free GalNAc and analyzed by flow cytometry. Results are expressed as the median of fluorescence ± SD (n = 3). The statistical significance is indicated compared to the results obtained in the absence of GalNAc. *: p < 0,05; **: p < 0,01.

GalNAc concentration resulted in a dose-dependent decrease in the median fluorescence of MGL ECD-Alexa Fluor 680. This competitive effect demonstrated that the MGL ECD binds to the cells through its carbohydrate recognition site, confirming its Tn-mediated cell surface recognition.

Detection of the Tn Antigen in HT29 Spheroids. We then investigated the capacity of MGL to penetrate deep cell layers by diffusion by evaluating whether it reached the center of 3D spheroids formed by HT29 cells. When live spheroids were incubated with MGL ECD-Alexa Fluor 680, the staining was intensely positive on the sphere periphery, and although some positive cells were also detected within the spheroids (Figure 4a), MGL ECD-Alexa Fluor 680 showed poor diffusion capacity through the HT29 cell layers. Interestingly, we can see that the Tn antigen was abundant and homogeneously distributed throughout the spheroids since the staining was homogeneously detected when the MGL ECD-Alexa Fluor 680 was incubated on thin sections of the spheroids (Figure 4b) rather than on the intact 3D structures (Figure 4a).

In Vivo Detection of Tumors. These encouraging *in vitro* results inspired us to investigate the capacity of MGL ECD-Alexa Fluor 680 to target subcutaneous tumors after intravenous injection in mice.

Before administration of MGL ECD-Alexa Fluor 680 *in vivo*, we first verified that MGL ECD-Alexa Fluor 680 did not bind to mouse blood cells and that it remained in the plasma (Supporting Figure S1). Moreover, after intravenous administration of MGL ECD-Alexa Fluor 680 (10 nmol in 200 μL), 5% of the injected dose remained in the plasma after 5 h, demonstrating very good bioavailability in solution (Supporting Figure S2). Furthermore, no sign of acute toxicity, such as pain, changes in skin and fur, loss of weight, or behavioral changes, was detected in any of the treated mice.

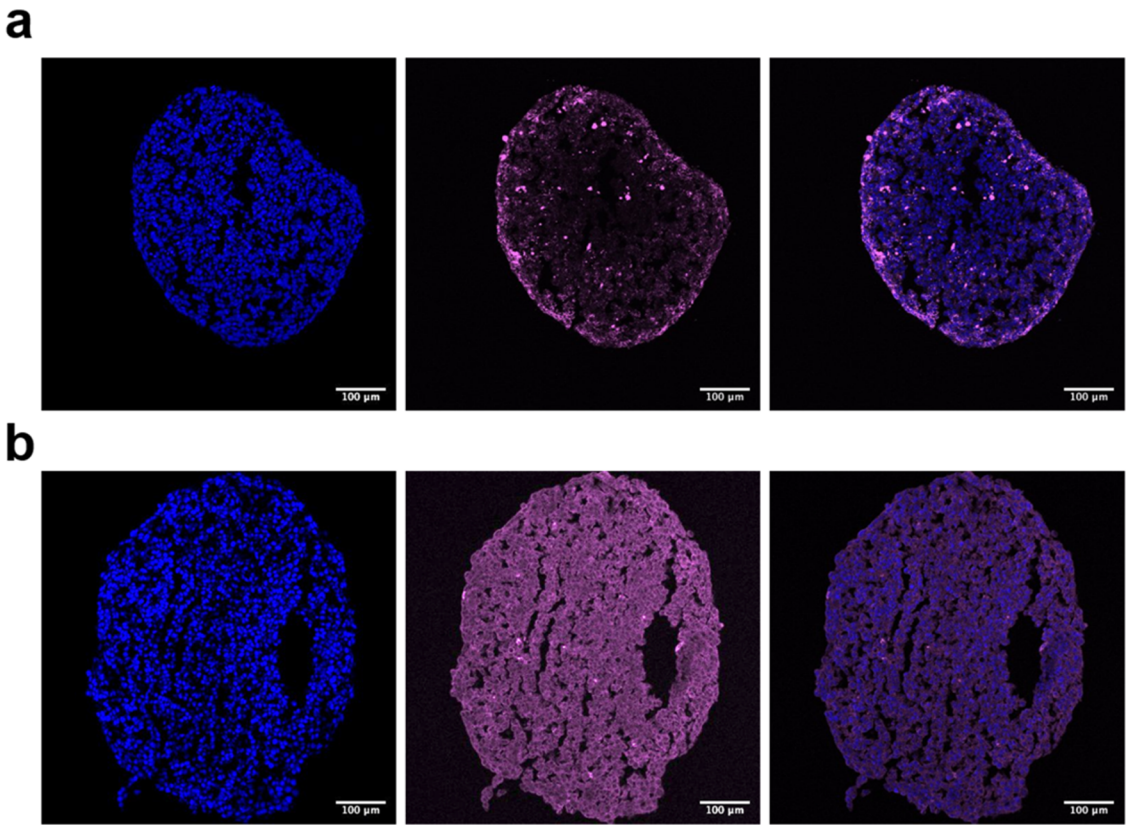

Figure 4. Labeling of HT29 spheroids with MGL ECD-Alexa Fluor 680. (a) Live spheroids were stained with MGL ECD-Alexa Fluor 680 before their fixation and sectioning. (b) HT29 spheroids were stained using MGL ECD-Alexa Fluor 680 after their sectioning, demonstrating the homogeneous presence of the Tn antigen throughout the spheroids. Left column (blue): images obtained using 5μM Hoechst 33342 staining of the DNA; middle column (magenta): Tn antigen detection using MGL-Alexa Fluor 680 staining; right column: overlay of the two colors.

https://doi.org/10.1021/acs.molpharmaceut.1c00744
Mol. Pharmaceutics XXXX, XXX, XXX−XXX

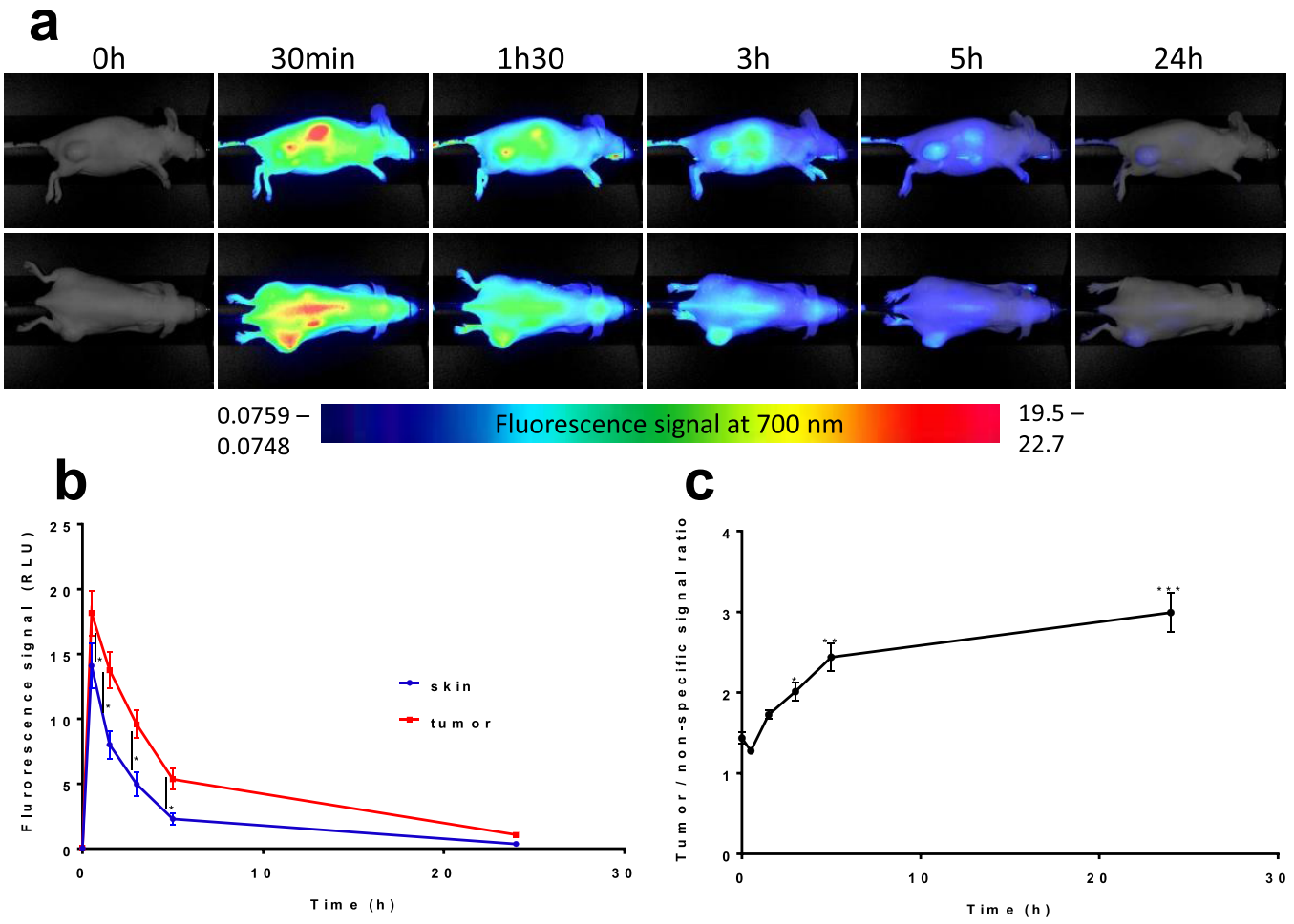

Figure 5. Representative fluorescence images of nude mice bearing HT29 subcutaneous tumors after intravenous injection of MGL ECD-Alexa Fluor 680 (10 nmol). (a) Images were recorded using 2D-fluorescence reflectance optical imaging (FRI) at 700 nm at different times after injection (min-max: dorsal view: 0.0759-19.5; side view: 0.0748-22.7). (b) Red line shows the mean ± SD fluorescence signal of tumor ROI, and blue line shows the mean ± SD non-specific signal present in the skin (n = 6). (c) Black line shows the mean ± SD tumor/skin fluorescence ratios. *: p < 0,05; **: p < 0,001; ***: p < 10-5 (n = 9).

MGL ECD-Alexa Fluor 680 was then administered intravenously in the tail vein of mice bearing HT29 subcutaneous tumors, and the fluorescence signal was followed in real time in live animals by fluorescence reflectance imaging. As shown in Figure 5, the fluorescence signal was distributed quite homogeneously in the body and started to accumulate in the subcutaneous tumors as well as in the kidneys and liver within 30 min of the injection. This fluorescence was then eliminated more rapidly from normal tissue (including skin) than from tumors, as indicated by the labeling intensity (Figure 5b), providing a tumor/skin ratio of >3 at 24 h (Figure 3c). Three mice were sacrificed after 5 h, and three others were sacrificed after 24 h; the fluorescence levels were measured in the organs extracted from these mice (Figure 6).

This result confirms the greater persistence of the fluorescent probe in the tumor tissues, as described above, than in normal tissues. Indeed, the fluorescence signal decreased more rapidly in all organs than in tumors. At 24 h, the subcutaneous tumors were the most fluorescent tissues, second to organs such as the liver and kidneys, indicating the detoxification of blood and elimination of the injected probe.

To rule out the possibility that the signal was caused solely by the passive enhanced permeability and retention (EPR) effect, not by active targeting, we injected purified bovine serum albumin (BSA) labeled with Alexa Fluor 680 into mice with HT29 tumors. We had previously shown that HT29 tumors can be classified as EPR-positive tumors[36] and that MGL ECD-Alexa Fluor 680 could thus significantly accumulate passively in tumors. As shown in Supporting Figure S3, the tumor/skin ratio was always lower than 2 with BSA, implicating the passive EPR effect only, but it was higher than 3 when MGL ECD-Alexa Fluor 680 was used. Since BSA and MGL ECD have similar MWs (60 and 90 kDa, respectively) and are both bioavailable for long periods after IV administration, we can thus assume that MGL ECD-Alexa Fluor 680 accumulation in tumors is efficient and involves active targeting.

To confirm the active targeting of tumor cells by MGL ECD-Alexa Fluor 680, HT29 tumor sections were examined by confocal microscopy after colabeling of vascular endothelial cells using an anti-CD31 antibody and Hoechst 33342 staining of nuclei (Figure 7).

We observed that MGL ECD-Alexa Fluor 680 (magenta) did not stain CD31$^+$ endothelial cells in contact with blood, as expected.[37] In contrast, MGL ECD-Alexa Fluor 680 accumulated on tumor cells, particularly those forming the first layers of a tumor immediately under the endothelium, confirming the active targeting of tumor cells.

https://doi.org/10.1021/acs.molpharmaceut.1c00744
Mol. Pharmaceutics XXXX, XXX, XXX−XXX

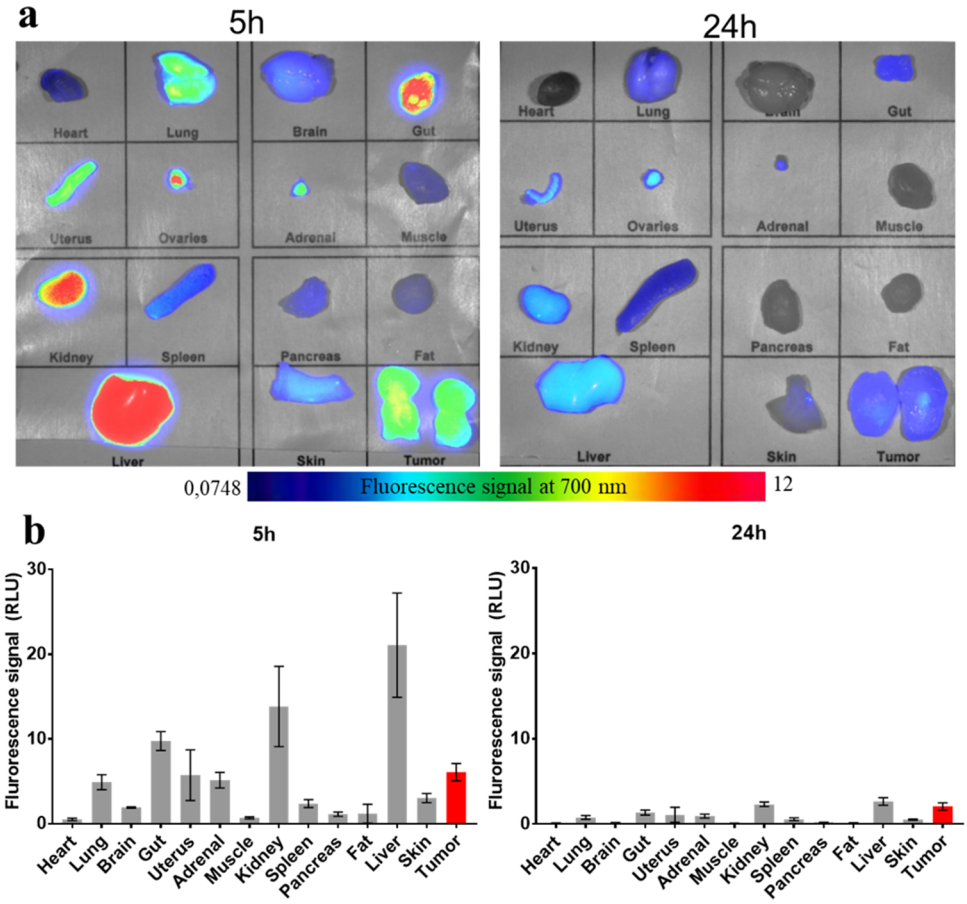

Figure 6. Fluorescence images were obtained on isolated organs 5 and 24 h after intravenous injection of MGL ECD-Alexa Fluor 680. (a) Representative fluorescence images of organs extracted from injected mice (min-max: 0.0748-12). (b) ROI was defined on the extracted organs to semiquantify the number of photons detected per pixel. The results are expressed as the mean ± SD in HT29 tumor-bearing mice (n = 3/time).

DISCUSSION

The development of efficient tumor-targeting compounds that can deliver contrast agents for diagnostics or drugs for therapeutic applications is still a major field of investigation.

After cloning and expressing the MGL extracellular domain (ECD) in *E. coli*, we showed the high avidity of MGL ECD for GalNAc (316 nM) using SPR. This avidity was strong enough to enable the detection of the Tn antigen expressed at low concentrations on A549 human lung cancer cells or at higher concentrations on HT29 human colon cancer cells. Importantly, no unspecific labeling was observed with Tn-negative tumor cells, such as H322 cells, a human lung cancer cell line. Using flow cytometry, we found that MGL ECD-Alexa Fluor 680 performs as well as the Bric111 anti-Tn antibody and seems to be slightly more sensitive than HPA, another lectin. Its specificity for GalNAc was confirmed using a competition assay in the presence of soluble GalNAc. Indeed, when the GalNAc concentration was increased, cell labeling by MGL ECD-Alexa Fluor 680 was decreased. This outcome demonstrates that the purified MGL ECD-Alexa Fluor 680 construct recognized Tn-positive tumor cells and GalNAc through the same recognition site.

In addition to its specific binding, MGL ECD-Alexa Fluor 680 diffused within the HT29 cell layers in spheroids, as indicated by some labeling found in the center of the 3D cell structures after 24 h of incubation. However, because of its preferential and strong binding on the first layers of HT29 cells, the fluorescent label was predominantly detected on the surface of the spheroids, even when the Tn antigen was homogeneously expressed by all of the cells. This result is in good agreement with our *in vivo* data showing that MGL efficiently labels Tn-positive tumor cells after passing passively through the leaky and Tn-negative tumor-induced neoendothelial cell layer.

MGL ECD-Alexa Fluor 680 plasma distribution and its low molecular weight (84 kDa), which is smaller than antibodies, were expected to contribute to its passive accumulation in tumors via the EPR effect, even without active targeting due to its recognition of Tn-positive cells. However, after intravenous injection of MGL ECD-Alexa Fluor 680, the tumor/skin ratio was clearly higher than that of a nontargeted protein such as BSA, confirming that MGL ECD-Alexa Fluor 680 is actively and specifically capable of tumor targeting *in vivo*. Notably, no particular toxicity was observed during the 24 h experiment time, and importantly, it did not bind to red blood cells.

The *ex vivo* results obtained with tumor sections confirmed the fluorescence reflectance imaging (FRI) analysis. A strong signal was found in the liver and kidneys, which indicated that MGL ECD-Alexa Fluor 680 was rapidly eliminated, particularly via hepatic filtration, but in addition to these two detoxification organs, the strongest signal was measured in tumors and, in particular, in the first layers composed of tumor cells in contact with blood vessels. No particular staining was detected by confocal microscopy in neoangiogenic or other blood vessels in tumor sections.

https://doi.org/10.1021/acs.molpharmaceut.1c00744
Mol. Pharmaceutics XXXX, XXX, XXX−XXX

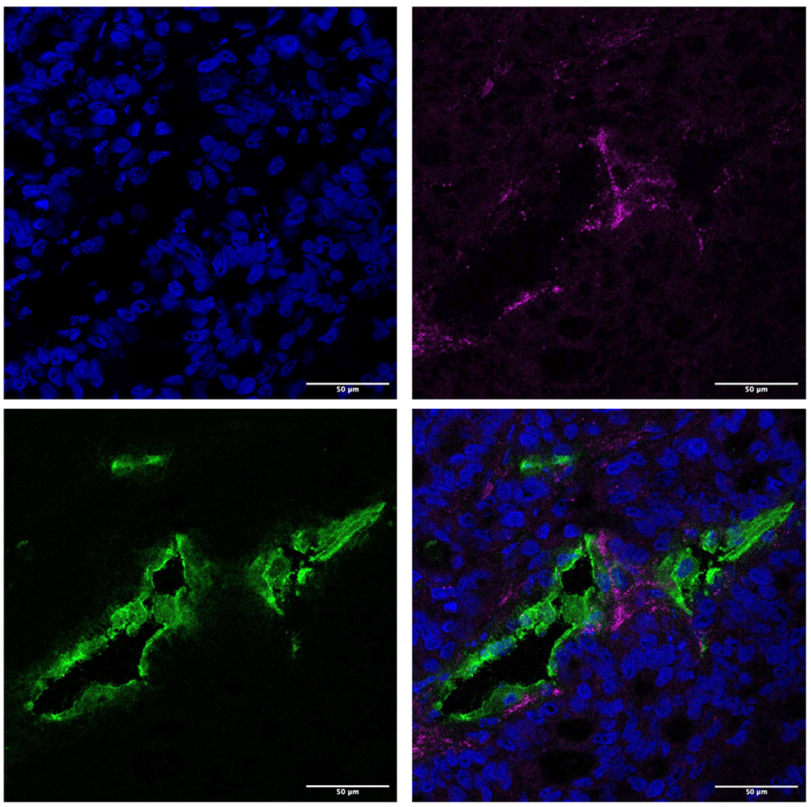

Figure 7. Confocal laser scanning microscopic images of HT29 subcutaneous tumors dissected 5 h after intravenous injection of 10 nmol of MGL ECD-Alexa680. Immunohistochemistry on frozen tumor sections with anti-CD31 (green) for endothelial cell labeling and Hoechst 33342 (blue) staining the cell nuclei. MGL ECD-Alexa680 (Magenta). Scale bar: 50 μm.

Current tumor-targeting ligands are usually directed against proteins overexpressed in cancer, such as integrins, the EGF receptor, and folate receptors.[38] In addition to these proteins, tumor-associated carbohydrate antigens (TACAs) are attracting increasing interest as possible targets, particularly the Tn antigen that can be overexpressed in cancer cells;[10,35] this antigen is currently recognized as a target for immunotherapy based on CAR T cells.[39]

The Tn antigen is recognized by antigen-presenting cells (dendritic cells and macrophages),[40] leading to the activation of complex immune responses. On the one hand, the administration of glycan-based therapies has been suggested for anticancer vaccination.[41,42] On the other hand, recognition of Tn-positive tumor cells by immune cells may result in immunosuppression,[43,44] by promoting Treg cell differentiation and favoring suppression of T cell activation. Exogenously administered purified MGL could thus be used to compete and reduce the binding of dendritic cells on the Tn-expressing tumor cells, and thus reducing tumor escape. In this aim, monoclonal anti-Tn antibodies are under development, but to date, most of the Tn-recognizing molecules are plant lectins.[45,46] Because of their plant origin, these lectins cannot be administered directly into humans without causing strong immune reactions. Our MGL ECD fragment should thus be considered a possible alternative for biomedical applications directed against the Tn antigen because of its human origin, physicochemical properties, bioavailability, and failure to induce acute toxicity. However, since our MGL is produced by *E. coli* without glycosylation, it will be necessary to verify its lack of immunogenicity. Should its lack of immunogenicity be confirmed, the MGL ECD fragment can be produced using mammalian cells.[11]

In conclusion, our study demonstrates the ability of MGL ECD to specifically target human tumors via the multivalent recognition of the Tn antigen frequently overexpressed in human tumors. This MGL ECD fragment extracted from a normal human protein presents an interesting tumor-targeting capacity, induces no acute toxicity, and is rapidly eliminated. Because of its human origin, it is not expected to induce a particular immune reaction. Altogether, MGL ECD is thus a vector candidate for the diagnosis and imaging of human tumors and, possibly, for targeted drug delivery.

■ ASSOCIATED CONTENT

Supporting Information

The Supporting Information is available free of charge at https://pubs.acs.org/doi/10.1021/acs.molpharmaceut.1c00744.

Blood and plasma distribution and tumor/skin ratios after intravenous administration of MGL ECD-Alexa Fluor 680 (PDF)

■ AUTHOR INFORMATION

Corresponding Authors

Franck Fieschi − *Univ. Grenoble Alpes, CNRS, CEA, Institut de Biologie Structurale, 38000 Grenoble, France*; Email: franck.fieschi@ibs.fr

Jean-Luc Coll − *Univ. Grenoble Alpes, INSERM U1209, CNRS UMR5309, Institute for Advanced Biosciences, 38000*

https://doi.org/10.1021/acs.molpharmaceut.1c00744
Mol. Pharmaceutics XXXX, XXX, XXX−XXX

Grenoble, France; orcid.org/0000-0002-2453-3552; Email: jean-luc.coll@univ-grenoble-alpes.fr

Authors

François Bulteau − *Univ. Grenoble Alpes, CNRS, CEA, Institut de Biologie Structurale, 38000 Grenoble, France; Univ. Grenoble Alpes, INSERM U1209, CNRS UMR5309, Institute for Advanced Biosciences, 38000 Grenoble, France; Univ. Grenoble Alpes, CNRS, Département de Chimie Moléculaire, UMR 5250, 38000 Grenoble, France*

Michel Thépaut − *Univ. Grenoble Alpes, CNRS, CEA, Institut de Biologie Structurale, 38000 Grenoble, France*

Maxime Henry − *Univ. Grenoble Alpes, INSERM U1209, CNRS UMR5309, Institute for Advanced Biosciences, 38000 Grenoble, France*

Amandine Hurbin − *Univ. Grenoble Alpes, INSERM U1209, CNRS UMR5309, Institute for Advanced Biosciences, 38000 Grenoble, France*

Laetitia Vanwonterghem − *Univ. Grenoble Alpes, INSERM U1209, CNRS UMR5309, Institute for Advanced Biosciences, 38000 Grenoble, France*

Corinne Vivès − *Univ. Grenoble Alpes, CNRS, CEA, Institut de Biologie Structurale, 38000 Grenoble, France*

Aline Le Roy − *Univ. Grenoble Alpes, CNRS, CEA, Institut de Biologie Structurale, 38000 Grenoble, France*

Christine Ebel − *Univ. Grenoble Alpes, CNRS, CEA, Institut de Biologie Structurale, 38000 Grenoble, France*

Olivier Renaudet − *Univ. Grenoble Alpes, CNRS, Département de Chimie Moléculaire, UMR 5250, 38000 Grenoble, France;* orcid.org/0000-0003-4963-3848

Complete contact information is available at: https://pubs.acs.org/10.1021/acs.molpharmaceut.1c00744

Author Contributions

F.B. and M.T. performed the MGL formulation, characterization, and *in vitro* study; analyzed the data; and wrote the manuscript with the guidance and support of F.F. and J-L.C. C.V. performed SPR characterization of the MGL constructs with F.B. A.H. and L.V. performed confocal microscopy studies. A.LR. and C.E. performed the AUC analysis. M.H. and F.B. performed the animal imaging and immunohistology study. O.R. F.F., and J-L. C conceived the project, designed the experiments, and analyzed the data.

Notes

The authors declare no competing financial interest.

■ ACKNOWLEDGMENTS

The authors thank the CDP Glyco@Alps (ANR-15-IDEX-02) for their financial support. The optimal imaging platform for 2DFRI Imaging was supported by France Life Imaging (French program "Investissement d'Avenir" grant; "Infrastructure d'avenir en Biologie Santé", ANR-11-INBS-0006) and the IBISA French consortium "Infrastructures en Biologie Santé et Agronomie". This work was based on the MP3 and AUC platforms at the Grenoble Instruct-ERIC center (ISBG; UMS 3518 CNRS-CEA-UGA-EMBL) within the Grenoble Partnership for Structural Biology, supported by FRISBI (ANR-10-INBS-05−02). The confocal microscope was partially funded by the Association for Research on Cancer, French Ministry "Enseignement Superieur et Recherche" and the Rhone-Alpes region (Contrat de projets Etat−Région 2007−2013 "Exploration du vivant, Imagerie biomedicale").

■ REFERENCES

(1) Varki, A. Evolutionary forces shaping the Golgi glycosylation machinery: why cell surface glycans are universal to living cells. *Cold Spring Harbor Perspect. Biol.* **2011**, *3*, No. a005462.

(2) Marth, J. D.; Grewal, P. K. Mammalian glycosylation in immunity. *Nat. Rev. Immunol.* **2008**, *8*, 874−887.

(3) Hakomori, S. Aberrant glycosylation in tumors and tumor-associated carbohydrate antigens. *Adv. Cancer Res.* **1989**, *52*, 257−331.

(4) Reily, C.; Stewart, T. J.; Renfrow, M. B.; Novak, J. Glycosylation in health and disease. *Nat. Rev. Nephrol.* **2019**, *15*, 346−366.

(5) Satomaa, T.; Heiskanen, A.; Leonardsson, I.; Ångström, J.; Olonen, A.; Blomqvist, M.; Salovuori, N.; Haglund, C.; Teneberg, S.; Natunen, J.; Carpén, O.; Saarinen, J. Analysis of the human cancer glycome identifies a novel group of tumor-associated N-acetylglucosamine glycan antigens. *Cancer Res.* **2009**, *69*, 5811−5819.

(6) Brooks, S. A. The involvement of Helix pomatia lectin (HPA) binding N-acetylgalactosamine glycans in cancer progression. *Histol. Histopathol.* **2000**, *15*, 143−158.

(7) Brockhausen, I. Mucin-type O-glycans in human colon and breast cancer: glycodynamics and functions. *EMBO Rep.* **2006**, *7*, 599−604.

(8) Lisowska, E. Tn antigens and their significance in oncology. *Acta Biochim. Pol.* **1995**, *42*, 11−7.

(9) Kakeji, Y.; Tsujitani, S.; Mori, M.; Maehara, Y.; Sugimachi, K. Helix pomatia agglutinin binding activity is a predictor of survival time for patients with gastric carcinoma. *Cancer* **1991**, *68*, 2438−2442.

(10) Laack, E.; Nikbakht, H.; Peters, A.; Kugler, C.; Jasiewicz, Y.; Edler, L.; Hossfeld, D. K.; Schumacher, U. Lectin histochemistry of resected adenocarcinoma of the lung: helix pomatia agglutinin binding is an independent prognostic factor. *Am. J. Pathol.* **2002**, *160*, 1001−1008.

(11) van Vliet, S. J.; van Liempt, E.; Saeland, E.; Aarnoudse, C. A.; Appelmelk, B.; Irimura, T.; Geijtenbeek, T. B. H.; Blixt, O.; Alvarez, R.; van Die, I.; van Kooyk, Y. Carbohydrate profiling reveals a distinctive role for the C-type lectin MGL in the recognition of helminth parasites and tumor antigens by dendritic cells. *Int. Immunol.* **2005**, *17*, 661−669.

(12) Geijtenbeek, T. B.; van Vliet, S. J.; Engering, A.; 't Hart, B. A.; van Kooyk, Y. Self- and nonself-recognition by C-type lectins on dendritic cells. *Annu. Rev. Immunol.* **2004**, *22*, 33−54.

(13) Steinman, R. M.; Hawiger, D.; Nussenzweig, M. C. Tolerogenic dendritic cells. *Annu. Rev. Immunol.* **2003**, *21*, 685−711.

(14) Zamri, N.; Masuda, N.; Oura, F.; Yajima, Y.; Nakada, H.; Fujita-Yamaguchi, Y. Effects of two monoclonal antibodies, MLS128 against Tn-antigen and 1H7 against insulin-like growth factor-I receptor, on the growth of colon cancer cells. *BioSci. Trends* **2012**, *6*, 303−312.

(15) Loureiro, L. R.; Carrascal, M. A.; Barbas, A.; Ramalho, J. S.; Novo, C.; Delannoy, P.; Videira, P. A. Challenges in Antibody Development against Tn and Sialyl-Tn Antigens. *Biomolecules* **2015**, *5*, 1783−1809.

(16) King, M. J.; Parsons, S. F.; Wu, A. M.; Jones, N. Immunochemical studies on the differential binding properties of two monoclonal antibodies reacting with Tn red cells. *Transfusion* **1991**, *31*, 142−149.

(17) Henry, N. L.; Hayes, D. F. Cancer biomarkers. *Mol. Oncol.* **2012**, *6*, 140−146.

(18) Pervin, M.; Koyama, Y.; Isemura, M.; Nakamura, Y. Plant Lectins in Therapeutic and Diagnostic Cancer Research. *Int. J. Plant Biol. Res.* **2015**, *3*, No. 1030.

(19) Chen, K.; Gentry-Maharaj, A.; Burnell, M.; Steentoft, C.; Marcos-Silva, L.; Mandel, U.; Jacobs, I.; Dawnay, A.; Menon, U.; Blixt, O. Microarray Glycoprofiling of CA125 improves differential diagnosis of ovarian cancer. *J. Proteome Res.* **2013**, *12*, 1408−1418.

(20) Drickamer, K. Two distinct classes of carbohydrate-recognition domains in animal lectins. *J. Biol. Chem.* **1988**, *263*, 9557−9560.

(21) Zelensky, A. N.; Gready, J. E. The C-type lectin-like domain superfamily. *FEBS J.* **2005**, *272*, 6179−6217.

(22) Heger, L.; Balk, S.; Lühr, J. J.; Heidkamp, G. F.; Lehmann, C. H. K.; Hatscher, L.; Purbojo, A.; Hartmann, A.; Garcia-Martin, F.; Nishimura, S. I.; Cesnjevar, R.; Nimmerjahn, F.; Dudziak, D. CLEC10A Is a Specific Marker for Human CD1c(+) Dendritic Cells and Enhances Their Toll-Like Receptor 7/8-Induced Cytokine Secretion. *Front. Immunol.* **2018**, *9*, No. 744.
(23) Marcelo, F.; Supekar, N.; Corzana, F.; van der Horst, J. C.; Vuist, I. M.; Live, D.; Boons, G. J. P. H.; Smith, D. F.; van Vliet, S. J. Identification of a secondary binding site in human macrophage galactose-type lectin by microarray studies: Implications for the molecular recognition of its ligands. *J. Biol. Chem.* **2019**, *294*, 1300−1311.
(24) Schwartz, A. L.; Steer, C. J.; Kempner, E. S. Functional size of the human asialoglycoprotein receptor as determined by radiation inactivation. *J. Biol. Chem.* **1984**, *259*, 12025−12029.
(25) Maalej, M.; Forgione, R. E.; Marchetti, R.; Bulteau, F.; Thépaut, M.; Lanzetta, R.; Laguri, C.; Simorre, J. P.; Fieschi, F.; Molinaro, A.; Silipo, A. Human Macrophage Galactose-Type Lectin (MGL) Recognizes the Outer Core of *Escherichia coli* Lipooligosaccharide. *ChemBioChem* **2019**, *20*, 1778−1782.
(26) Halary, F.; Amara, A.; Lortat-Jacob, H.; Messerle, M.; Delaunay, T.; Houlès, C.; Fieschi, F.; Arenzana-Seisdedos, F.; Moreau, J. F.; Déchanet-Merville, J. Human cytomegalovirus binding to DC-SIGN is required for dendritic cell infection and target cell trans-infection. *Immunity* **2002**, *17*, 653−664.
(27) Zhao, H.; Ghirlando, R.; Piszczek, G.; Curth, U.; Brautigam, C. A.; Schuck, P. Recorded scan times can limit the accuracy of sedimentation coefficients in analytical ultracentrifugation. *Anal. Biochem.* **2013**, *437*, 104−108.
(28) Schuck, P. Size-distribution analysis of macromolecules by sedimentation velocity ultracentrifugation and lamm equation modeling. *Biophys. J.* **2000**, *78*, 1606−1619.
(29) Brautigam, C. A. Calculations and Publication-Quality Illustrations for Analytical Ultracentrifugation Data. *Methods Enzymol.* **2015**, *562*, 109−133.
(30) Philo, J. S. An improved function for fitting sedimentation velocity data for low-molecular-weight solutes. *Biophys. J.* **1997**, *72*, 435−444.
(31) Suzuki, N.; Yamamoto, K.; Toyoshima, S.; Osawa, T.; Irimura, T. Molecular cloning and expression of cDNA encoding human macrophage C-type lectin. Its unique carbohydrate binding specificity for Tn antigen. *J. Immunol.* **1996**, *156*, 128−135.
(32) Jégouzo, S. A.; Quintero-Martinez, A.; Ouyang, X.; dos Santos, A.; Taylor, M. E.; Drickamer, K. Organization of the extracellular portion of the macrophage galactose receptor: a trimeric cluster of simple binding sites for N-acetylgalactosamine. *Glycobiology* **2013**, *23*, 853−64.
(33) Lescar, J.; Sanchez, J. F.; Audfray, A.; Coll, J. L.; Breton, C.; Mitchell, E. P.; Imberty, A. Structural basis for recognition of breast and colon cancer epitopes Tn antigen and Forssman disaccharide by Helix pomatia lectin. *Glycobiology* **2007**, *17*, 1077−1083.
(34) Schumacher, U.; Adam, E. Lectin histochemical HPA-binding pattern of human breast and colon cancers is associated with metastases formation in severe combined immunodeficient mice. *Histochem. J.* **1997**, *29*, 677−684.
(35) Pirro, M.; Rombouts, Y.; Stella, A.; Neyrolles, O.; Burlet-Schiltz, O.; van Vliet, S. J.; de Ru, A. H.; Mohammed, Y.; Wuhrer, M.; van Veelen, P. A.; Hensbergen, P. J. Characterization of Macrophage Galactose-type Lectin (MGL) ligands in colorectal cancer cell lines. *Biochim. Biophys. Acta, Gen. Subj.* **2020**, *1864*, No. 129513.
(36) Karageorgis, A.; Dufort, S.; Sancey, L.; Henry, M.; Hirsjärvi, S.; Passirani, C.; Benoit, J. P.; Gravier, J.; Texier, I.; Montigon, O.; Benmerad, M.; Siroux, V.; Barbier, E. L.; Coll, J. L. An MRI-based classification scheme to predict passive access of 5 to 50-nm large nanoparticles to tumors. *Sci. Rep.* **2016**, *6*, No. 21417.
(37) Wu, Z. L.; Person, A. D.; Anderson, M.; Burroughs, B.; Tatge, T.; Khatri, K.; Zou, Y.; Wang, L.; Geders, T.; Zaia, J.; Sackstein, R. Imaging specific cellular glycan structures using glycosyltransferases via click chemistry. *Glycobiology* **2018**, *28*, 69−79.
(38) Coll, J. L.; Choi, J. Challenges of Applying Targeted Nanostructures with Multifunctional Properties in Cancer Treatments. In *Nanoscience and Nanothechnology for Human Health*; Van de Voorde, M., Ed.; John Wiley & Sons, 2017; pp 127−156.
(39) Posey, A. D., Jr.; Schwab, R. D.; Boesteanu, A. C.; Steentoft, C.; Mandel, U.; Engels, B.; Stone, J. D.; Madsen, T. D.; Schreiber, K.; Haines, K. M.; Cogdill, A. P.; Chen, T. J.; Song, D.; Scholler, J.; Kranz, D. M.; Feldman, M. D.; Young, R.; Keith, B.; Schreiber, H.; Clausen, H.; Johnson, L. A.; June, C. H. Engineered CAR T Cells Targeting the Cancer-Associated Tn-Glycoform of the Membrane Mucin MUC1 Control Adenocarcinoma. *Immunity* **2016**, *44*, 1444−1454.
(40) Napoletano, C.; Zizzari, I. G.; Rughetti, A.; Rahimi, H.; Irimura, T.; Clausen, H.; Wandall, H. H.; Belleudi, F.; Bellati, F.; Pierelli, L.; Frati, L.; Nuti, M. Targeting of macrophage galactose-type C-type lectin (MGL) induces DC signaling and activation. *Eur. J. Immunol.* **2012**, *42*, 936−945.
(41) Anderluh, M.; Berti, F.; Bzducha-Wróbel, A.; Chiodo, F.; Colombo, C.; Compostella, F.; Durlik, K.; Ferhati, X.; Holmdahl, R.; Jovanovic, D.; Kaca, W.; Lay, L.; Marinovic-Cincovic, M.; Marradi, M.; Ozil, M.; Polito, L.; Reina, J. J.; Reis, C. A.; Sackstein, R.; Silipo, A.; Svajger, U.; Vanek, O.; Yamamoto, F.; Richichi, B.; van Vliet, S. J. Recent advances on smart glycoconjugate vaccines in infections and cancer. *FEBS J.* **2021**, DOI: 10.1111/febs.15909.
(42) Asín, A.; García-Martín, F.; Busto, J. H.; Avenoza, A.; Peregrina, J. M.; Corzana, F. Structure-based Design of Anti-cancer Vaccines: The Significance of Antigen Presentation to Boost the Immune Response *Curr. Med. Chem.* 2021, *28*, DOI: 10.2174/0929867328666210810152917.
(43) da Costa, V.; van Vliet, S. J.; Carasi, P.; Frigerio, S.; Garcia, P. A.; Croci, D. O.; Festari, M. F.; Costa, M.; Landeira, M.; Rodriguez-Zraquia, S. A.; Cagnoni, A. J.; Cutine, A. M.; Rabinovich, G. A.; Osinaga, E.; Marino, K. V.; Freire, T. The Tn antigen promotes lung tumor growth by fostering immunosuppression and angiogenesis via interaction with Macrophage Galactose-type lectin 2 (MGL2). *Cancer Lett.* **2021**, *518*, 72−81.
(44) van Kooyk, Y.; Ilarregui, J. M.; van Vliet, S. J. Novel insights into the immunomodulatory role of the dendritic cell and macrophage-expressed C-type lectin MGL. *Immunobiology* **2015**, *220*, 185−192.
(45) He, Y.; Schreiber, K.; Wolf, S. P.; Wen, F.; Steentoft, C.; Zerweck, J.; Steiner, M.; Sharma, P.; Shepard, H. M.; Posey, A.; June, C. H.; Mandel, U.; Clausen, H.; Leisegang, M.; Meredith, S. C.; Kranz, D. M.; Schreiber, H. Multiple cancer-specific antigens are targeted by a chimeric antigen receptor on a single cancer cell *JCI Insight* 2019, *421* DOI: 10.1172/jci.insight.130416.
(46) Poiroux, G.; Barre, A.; van Damme, E. J. M.; Benoist, H.; Rouge, P. Plant Lectins Targeting O-Glycans at the Cell Surface as Tools for Cancer Diagnosis, Prognosis and Therapy. *Int. J. Mol. Sci.* **2017**, *18*, No. 1232.

https://doi.org/10.1021/acs.molpharmaceut.1c00744
Mol. Pharmaceutics XXXX, XXX, XXX−XXX